Ultraviolet emission and Fano resonance in doped nano-alumina

Bin Li, Samuel L. Oliveira, and Stephen C. Rand[a)]
Electrical Engineering and Computer Science Department, University of Michigan, Ann Arbor, Michigan 48109-2122

Jose A. Azurdia, Tom R. Hinklin, Julien C. Marchal, and Richard M. Laine
Department of Materials Science and Engineering, University of Michigan, Ann Arbor, Michigan 48109-2136

(Received 18 September 2006; accepted 28 December 2006; published online 15 March 2007)

Emission properties of Al_2O_3 nanopowders, synthesized by flame spray pyrolysis with Mg, Cr, and Sc dopants, are investigated, principally in the protein lysing range of 250–290 nm (UV-C band). As expected, point defect densities depend on crystal phase and irradiation history and strongly influence emission properties at short wavelengths. Ultraviolet and visible emission intensities of aggregated point defect centers change upon electron beam exposure at high current densities, but ultraviolet emission from point defects is persistently enhanced over a narrow range of Mg-doped Al_2O_3 compositions slightly off spinel stoichiometry. At 40% Mg concentration, emission intensities at 320 nm rise by over an order of magnitude after beam exposure. Quantum efficiency for cathodoluminescence in the 250–300 nm range nevertheless remains low. Point defect ionization at high currents shifts the emission of Al_2O_3 nanopowders to the infrared and is shown to be correlated with a ubiquitous Fano resonance in ionized Cr-vacancy complexes. This base line spectroscopy permits us to attribute the very high quantum efficiency of UV-C luminescence in annealed $Sc^{3+}:Al_2O_3$ primarily to the formation of α-phase Al_2O_3. © *2007 American Institute of Physics*. [DOI: 10.1063/1.2496514]

I. INTRODUCTION

Following a century of active research on the optical properties of semiconductors and dielectrics containing rare earth impurities, transition metals, alkalis, and other dopants that are useful for displays and medical imaging,[1] optimized phosphors that can be excited by high energy photons or particles are now commercially available for displays, imagers, and biosensors throughout the visible spectral region. Visible (upconversion) phosphors that are excited in the infrared by low energy photons are used routinely for sensitive bioassays.[2] Research continues to target new materials for improved efficiencies, longer lifetimes, and better CIE color indices,[3] but virtually all efforts are focused on visible emitters. Similarly, research on x-ray scintillators has sought to optimize the conversion efficiency from x-rays to visible photons. In contrast, research on crystalline solids that emit light in the UV-C range of 250–290 nm has been and still is scant, because this range is not directly useful for lighting, displays, or scintillators. Radiation in this range is invisible and few solids either generate or transmit light efficiently at such short wavelengths.

Nevertheless, radiation in the UV-C spectral range of 250–290 nm overlaps key protein absorption bands[4] and causes damage to protein linkages.[5] Efficient UV phosphors in this range can potentially serve not only as components for therapeutics or sterilization units but also to deliver UV-C radiation in design geometries or sizes that are impractical for the mercury vapor discharge lamps customarily used in water purification systems. Phosphor processing into ultraviolet-emitting thin films or transparent ceramic sheets could also offer new approaches to decontamination technology that would avoid the hazardous use of mercury and provide durable, long-lasting emitters. In small systems such as micro- and nanofluidic on-chip analyzers,[6] electrically pumped, solid-state UV-C emitters compatible with oxide hosts that exhibit excellent chemical resistance, physical robustness, and radiation hardness could also provide unique functionality for protein chromatography.

The successful synthesis of optical ceramics of very high quality would also enable the development of tunable laser sources in the UV-C range. There are only a few candidates for solids that could emit ultraviolet radiation efficiently enough to replace high flux mercury sources. The possibilities include dielectrics containing high concentrations of stable, intrinsic point defects, dielectrics doped with radiative impurities, and wide band gap semiconductors. Here we consider the first and second of these possibilities, focusing initially on anion vacancies in alumina that are compact enough to have energy levels in the desired range[7,8] and subsequently on Sc impurities which have broad optical transitions in the ultraviolet. We show that in Sc-doped alumina, efficient impurity UV-C luminescence can be achieved by minimizing color center concentration and controlling the alumina phase.

Defect centers in alumina are relatively stable due to the covalent nature of the oxide host and generally have high oscillator strengths. So they are of interest both as potential modifiers of impurity emission and as primary emitters. Here, we first investigate oxygen vacancy centers with short wavelength transitions that are found to occur in high concentrations in as-grown alumina nanopowders, synthesized by liquid-feed flame spray pyrolysis (LF-FSP) under condi-

a)Electronic mail: scr@umich.edu

tions far from thermal equilibrium.[9] The presence of such centers is in itself unusual, since corundum is reputedly a radiation-hard material.[10] These defects exhibit cathodoluminescence (CL) that partly overlaps the range of interest (250–290 nm). Their emission can be shifted to shorter wavelengths with MgO doping and partly stabilized through charge compensation and electron beam processing. Here we report some of these properties. A Fano resonance is identified in alumina that is helpful in monitoring defect concentrations and dynamics due to its proportionality to the density of IR-emitting centers. However, defect-related emission of $MgO:Al_2O_3$ in the UV-C range is ultimately shown to account for only a small proportion of the cathodoluminescence of this material, particularly at high currents where visible and infrared emissions become intense. Indeed infrared emission accounts for most of the radiative quantum efficiency and it has been proposed for laser applications in irradiated single crystals.[11] Hence native defects in LF-FSP oxides such as alumina have limited promise for simple, high intensity UV-C sources.

Optical spectroscopy of the defects in alumina nanopowders nevertheless facilitates an understanding of the ultraviolet emission properties of LF-FSP alumina doped with scandium. Although Sc^{3+} has a high quantum efficiency for broad emission in the UV-C range in crystalline α Al_2O_3,[12] its intensity is disappointingly weak in as-grown alumina powders despite the crystalline nature (δ phase) of individual nanoparticles. A key result of the present work is the finding that Sc^{3+} emission intensity improves by many orders of magnitude upon annealing at 1200 °C, a procedure that induces formation of the α phase.[13] After high temperature annealing, the absorption and emission of color centers as well as the intensity of the Fano resonance associated with them changed very little, but the scandium UV-C emission intensity increased by two orders of magnitude. Consequently, this procedure identifies a route for synthesizing nanocrystalline emitters with acceptable radiative performance over the entire UV-C band. This advance may make it possible to produce transparent $Sc^{3+}:Al_2O_3$ nanoceramic solids, a robust class of bulk solid ultraviolet emitters that might be useful for decontamination and solid state laser applications.

II. EXPERIMENTAL METHODS

Liquid-feed flame spray pyrolysis was used to prepare all samples for this study. Combinatorial synthesis of Al_2O_3 by this method has been described in detail previously.[14] Unaggregated single crystal nanoparticles with average diameters in the 30 nm range can be produced with this approach at rates in excess of 200 g/h, and for the present experiments $Mg_xAl_{2-x}O_3$ powders were prepared at 20 concentrations between $x=0.0$ and 0.5. The composition and phase of all samples were determined using x-ray diffraction (XRD). Representative XRD traces are given in Fig. 1, illustrating the remarkable degree of phase variation and control achievable by LF-FSP through variation of MgO content, despite the rapid quench and kinetic nature of the synthesis. At low Mg concentration the indexed x-ray patterns revealed a mixture of orthorhombic, tetragonal, and monoclinic phases. At intermediate MgO concentration the nanopowders were almost entirely of the tetragonal phase. At high concentration (>10% Mg) the dominant phase was found to be spinel ($MgAl_2O_4$). $Sc^{3+}:Al_2O_3$ nanopowders were also prepared at concentrations of 1 and 20 mol % Sc.

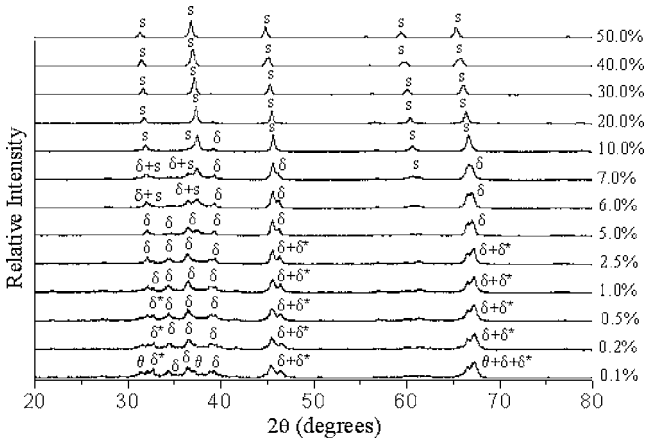

FIG. 1. X-ray diffraction patterns of LF-FSP $MgO:Al_2O_3$ powders. Below 2 mol % MgO, indexing revealed that samples were mixtures of orthorhombic (δ^*), tetragonal (δ), and monoclinic (θ) phases. The 5 mol % MgO sample was nearly pure tetragonal. Above ~10 mol% MgO, samples were primarily cubic and corresponded to the spinel (s) structure with 50% MgO composition ($MgAl_2O_4$).

As-grown samples were loaded onto oxygen-free copper stages in an ultrahigh vacuum chamber equipped with a high voltage electron gun and optical ports. Lightly compressed powders were subjected to 6 keV electron beams at currents ranging from 1 to 50 μA in a 1–2 mm spot in order to perform optical spectroscopy. Reproducibility was better than ± 1 μA when the acceleration voltage was held constant and the current was varied in gate-controlled mode. Luminescence was collected through a CaF_2 window and analyzed with 0.25 and 1.0 m grating spectrometers using photomultipliers and standard photon-counting electronics. In all, 36 optical scans were taken over wide spectral ranges in samples of Mg-doped alumina nanopowders. The grating sine drive advanced the wavelength by 0.1 nm under computer control every 4 s with 1 s averaging of the input signal. Observations were limited to wavelengths in the range of 200–800 nm by detector photocathode response. All CL spectra were obtained at vacuum levels below 5×10^{-9} Torr and represent repeatable, steady-state spectra, free of beam-induced outgassing effects, intersample contamination, or space charge effects inside the chamber. Spectra were not corrected in the important range of 200–300 nm because the detector response was flat and the UV grating was blazed for 250 nm.

Three CL spectra were recorded for each sample. The first was a low current scan at 3.5 μA, recorded as a reference spectrum for pristine samples. Figure 2 shows a set of spectra measured in this way. Following the low current irradiation, a second set of spectra was recorded at an elevated current level of 21.9 μA. Red and infrared emissions were observed to strengthen significantly with respect to the ultraviolet under these conditions, as shown in Fig. 3. Finally, a

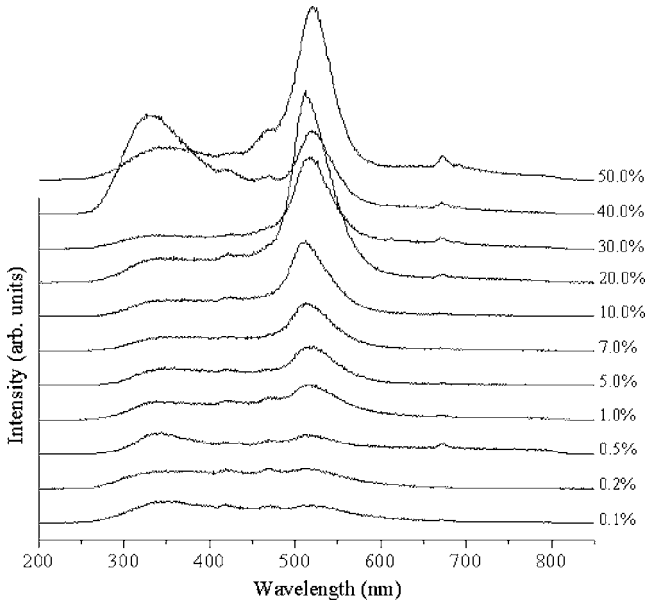

FIG. 2. Reference cathodoluminescence spectra of as-grown $MgO:Al_2O_3$ nanopowders containing various concentrations of MgO, taken at 6 keV with low current (3.5 μA).

third set of data (Fig. 4) was recorded for all samples by returning to the reference current level of 3.5 μA, reproducing the conditions but not the sample history of data in Fig. 2. Then, assignments of known color center peaks in alumina were made according to the peak positions indicated in Fig. 5(a). CL spectra of $Sc^{3+}:Al_2O_3$ samples were also recorded over the 200–800 nm spectral range (Fig. 6).

III. RESULTS

Cathodoluminescence spectroscopy over a wide range, including the visible and near infrared spectral regions, provides important perspective on optical dynamics in LF-FSP samples. Significant changes were induced by electron beam

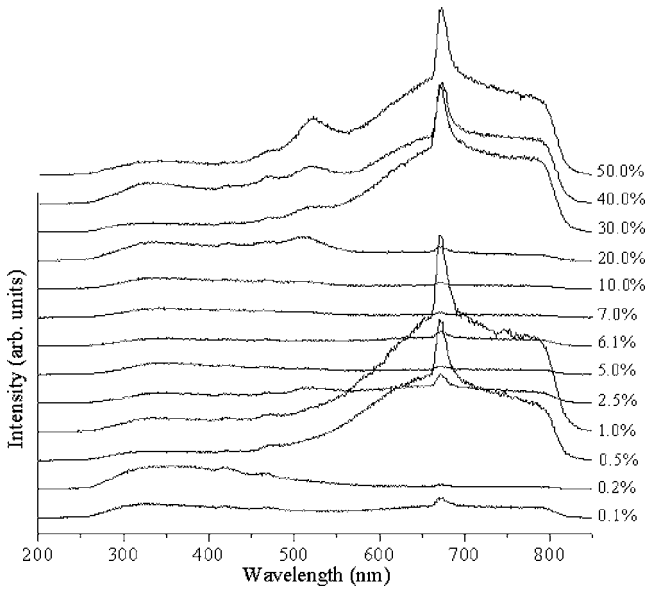

FIG. 3. Cathodoluminescence spectra of $MgO:Al_2O_3$ nanopowders recorded at 6 keV with high current (22 μA).

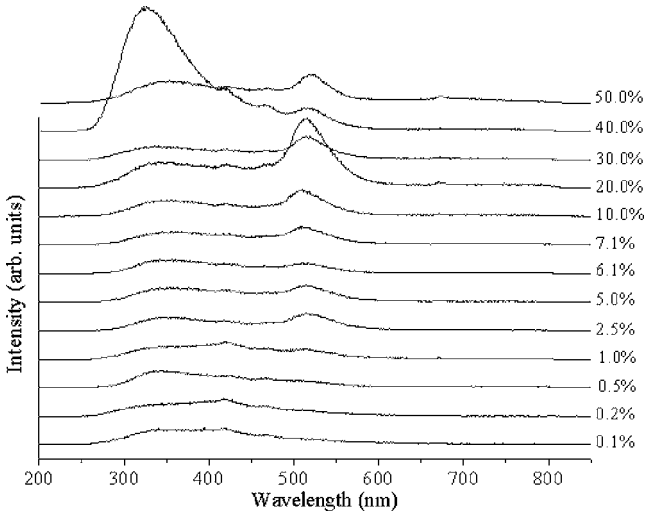

FIG. 4. Cathodoluminescence spectra $MgO:Al_2O_3$ nanopowders rerecorded at 6 keV with low current (3.5 μA) after beam processing for 30 min at 22 μA.

irradiation. We first analyze long wavelength features of the alumina data in Figs. 2–4, using assignments indicated in Fig. 5(a). We then discuss ultraviolet characteristics, including the emission of samples doped with scandium. A promi-

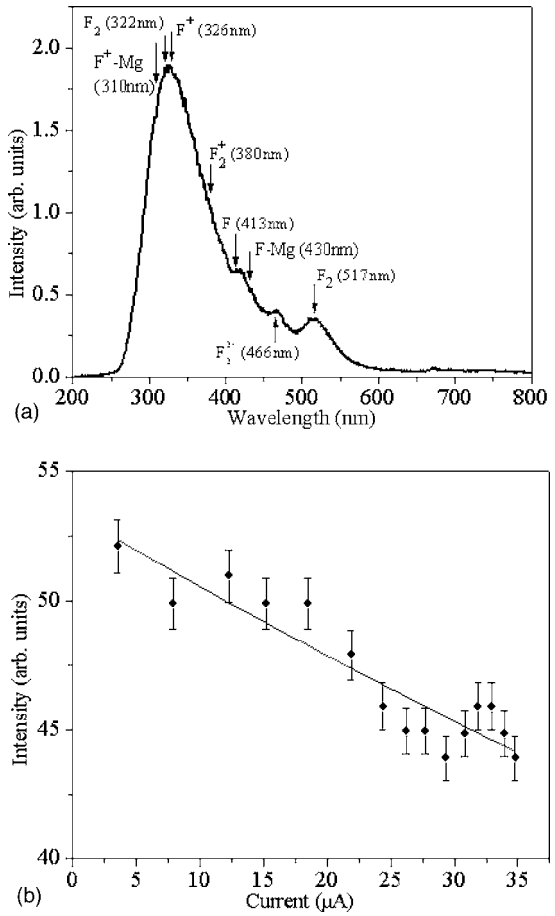

FIG. 5. (a) Cathodoluminescence spectrum of 40 mol % $MgO:Al_2O_3$ nanopowder showing emission peaks due to intrinsic point defects. (b) Intensity vs beam current of a circularly polarized He–Ne laser probe reflected from undoped Al_2O_3 nanopowder and detected with a helicity-preserving analyzer to eliminate the specular component.

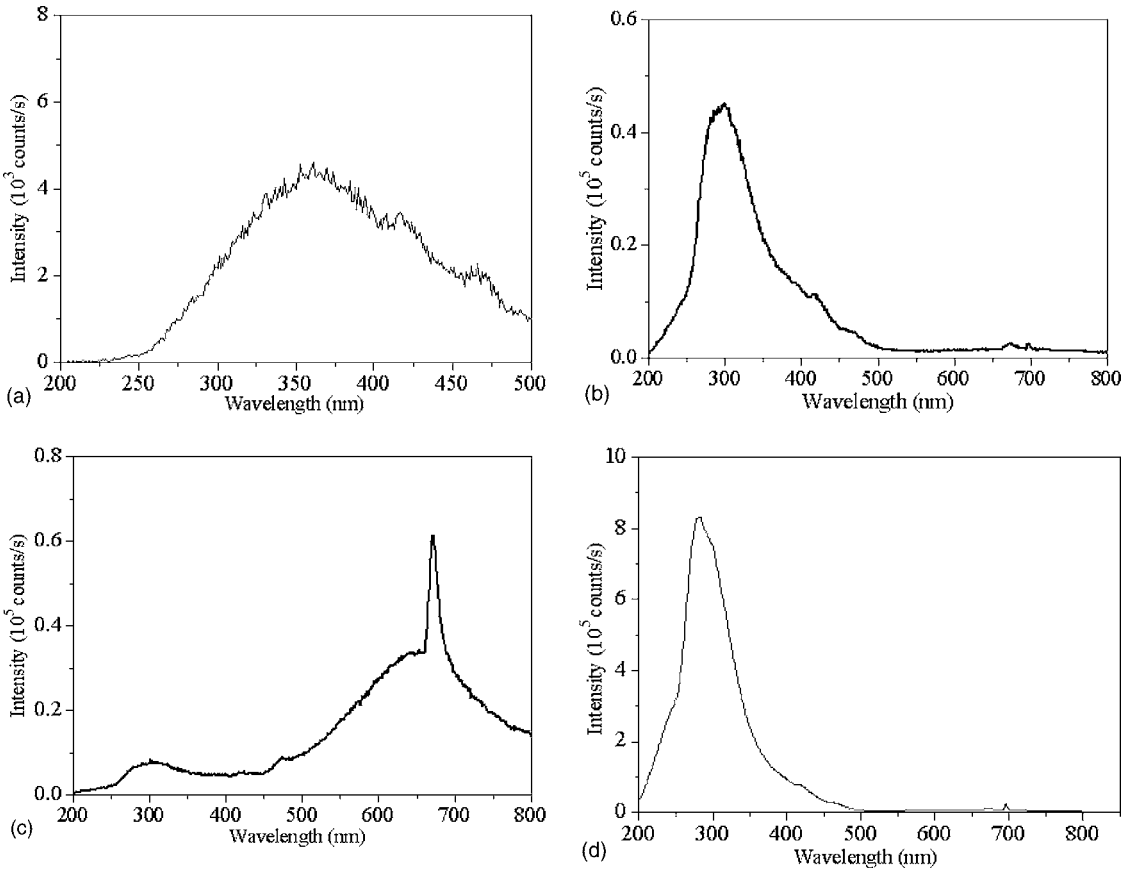

FIG. 6. Comparative CL emission spectra at 6 keV and 3.5 μA in (a) an unannealed sample of 20% $Sc^{3+}:Al_2O_3$ nanopowder (bottom trace) (b) a 20% $Sc^{3+}:Al_2O_3$ sample annealed at 1200 °C (top) and again excited with 3.5 μA (c) the same 20% $Sc^{3+}:Al_2O_3$ annealed sample excited at high current (21.9 μA), and finally (d) a 1% $Sc^{3+}:Al_2O_3$ sample annealed at 1200 °C excited at 3.5 μA.

nent spectral feature at 672 nm that appears in all powder samples is identified and shown to track the concentration of infrared point defects in these materials.

Emission wavelengths of simple oxygen vacancy centers in alumina and their aggregates are indicated in Fig. 5(a). This figure presents a typical CL spectrum of nanopowder synthesized by LF-FSP. In pristine samples, surprisingly intense emission is observed at 520 nm from intrinsic F_2 centers (Fig. 2). These centers consist of a pair of adjacent oxygen vacancies, each of which is occupied by two electrons,[10] and normally form only upon irradiation with intense ionizing radiation. Evidently, neutral divacancies of this type form during the rapid thermal quenching step following combustion and are abundant in LF-FSP samples. The emission intensity at 520 nm can be observed to drop dramatically during subsequent irradiation as the F_2 centers ionize to form F_2^+, F_2^{2+}, etc. (Fig. 3). Direct evidence for the generation of ionized centers is provided by the drop in reflectance of circularly polarized probe laser light at 632.8 nm as electron irradiation of the probe spot on the sample intensifies [Fig. 5(b)]. By probing the F_2^+ absorption region and selecting the same circular polarization at the detector as the incident beam (the helicity-preserving channel), only the signal light that has undergone multiple scattering in the interior of the sample is detected. Specular reflections from the surface are rejected with this approach, since their polarization is orthogonal to the analyzer. The drop in signal evident in Fig. 5(b) as the current increases therefore reflects a genuine increase of the number of absorbing centers in the sample interior. Charged states of more complex aggregates may also form at elevated currents and give rise to spectral features at wavelengths in the 550–1000 nm range (see Fig. 3) but have not been studied adequately to be assigned to specific point defect structures reliably.

Point defects consisting of single electrons occupying anion vacancies in alkali halide crystals have intrinsically high quantum efficiencies and are well understood.[15] Two-electron centers in oxides are comparatively poorly characterized but can also have very fast decay rates with quantum efficiencies approaching unity if intersystem crossing is slow. For example, the F^+ center has an oscillator strength of 0.8 in MgO (Ref. 16) and a decay time of 50 ns in Al_2O_3 (Ref. 17) at a wavelength of 325 nm,[18] indicating high radiative efficiency for this simple one-electron center in these hosts. Basic characteristics of F centers and Mg-modified centers in alumina are listed in Table I, where it can also be seen that the center wavelength of F^+ emission shifts when a neighboring cation is changed. For example, the emission peak shifts from 325 to 310 nm (Refs. 8 and 18) when Mg occupies a neighboring site.

F^+ centers with Mg^{2+} on a nearest neighbor site (designated as F^+-Mg in this paper) are therefore intriguing candidates for ultraviolet emission in LF-FSP powders, as reflected in the spectra of Figs. 2–4. Emission at 290 nm arises

TABLE I. Absorption and emission of point defects in sapphire.

Material	Defect symbol	Absorption peak (nm)	Emission peak (nm)
Al_2O_3	F	205	420[a]
$Mg:Al_2O_3$	F^+-Mg	255	310[b]
Al_2O_3	F^+	258	325[a]
Al_2O_3	F_2	300	322[a]
		300	517[c]
Al_2O_3	F_2^+	355	379[a]
		685	756[d]
Al_2O_3	F_2^{2+}	285	440[e]
		455	550[a]

[a]Reference 7.
[b]Reference 8.
[c]Reference 10.
[d]Reference 25.
[e]Reference 26.

from the recombination of holes with F^+-Mg centers which have a high cross section for hole recombination. In fact, the F^+-Mg cross section is thought to be higher than that of isolated F^+ centers.[8]

Recombination of ionized oxygen vacancy centers with holes or with electrons therefore readily decreases the density of F^+-Mg and F^+ centers when samples are subjected to ionizing radiation. Qualitatively, the small drop in ultraviolet intensity observed from 280 to 350 nm during high current irradiation of samples with Mg concentrations from 0.5% to 50% (Fig. 3) can be accounted for on this basis.

The broad (multicomponent) peak at 320 nm is ten times more intense in 40% $Mg:Al_2O_3$ than in any other composition. Moreover it intensifies by an additional 30% after high current irradiation with the electron beam. Although its spectral components are not resolved, this behavior suggests that in the 40% sample the joint concentration of neutral F centers and Mg impurity sites reaches a maximum, due to slight off stoichiometry with respect to perfect spinel composition. If the density of alternative electron traps also remains high, the ionization of F-Mg centers during high current beam irradiation may result in an increased density of persistently ionized F^+-Mg centers emitting in this range. Uncontrolled variations in the powder synthesis cannot be ruled out as a contributing factor to this anomaly, but the grouping of prominent defect spectra in Fig. 3 around MgO-dopant concentrations of 1% and 40% where important phase transformations take place supports the interpretation given above.

In Figs. 6(a) and 6(b), emission spectra of as-grown and annealed Al_2O_3 nanopowders doped with Sc^{3+} are shown. The broad peak at 280 nm in Fig. 6(b), absent in reference spectra of unannealed samples such as Fig. 6(a), is attributed to Sc^{3+} ions on the basis of prior spectroscopy in the α phase.[12] In the annealed sample, aggregate color centers of the host account only for a low intensity background observable at wavelengths longer than approximately 325 nm. The 672 nm resonance is also present but no more or less intense than before at high currents [Fig. 6(c)]. The main result to note is that the Sc^{3+} emission intensifies by at least two orders of magnitude upon annealing.

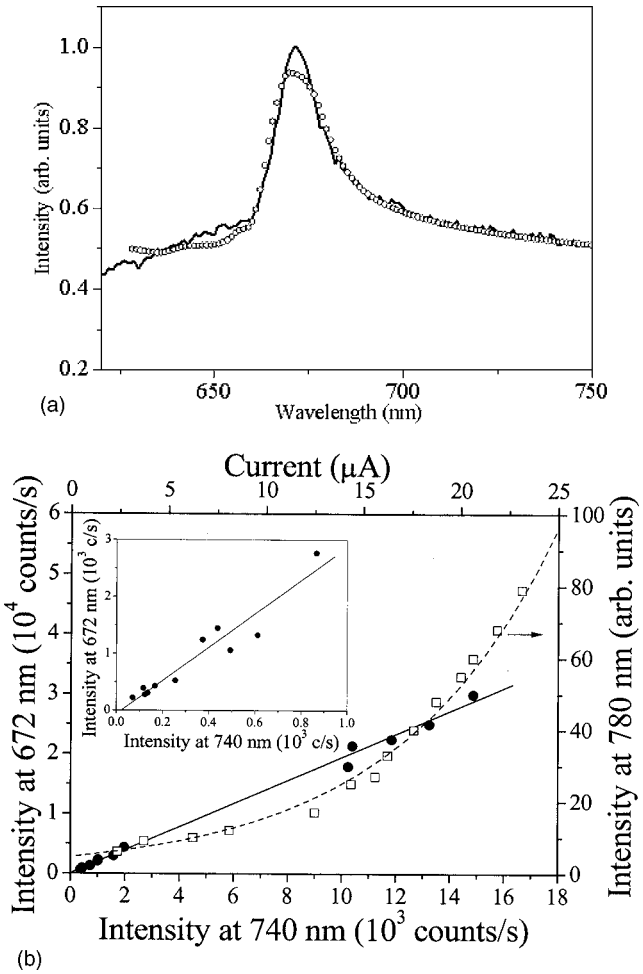

FIG. 7. (a) Calculation of Fano profile and comparison with the high current spectrum of $Mg:Al_2O_3$ in Fig. 3. (b) Ratios from Figs. 2 and 3 of the Fano peak height to background continuum intensity at various Mg concentrations and currents (solid circles). Also shown is background intensity at 780 nm versus current (open squares).

Infrared spectra near 672 nm in Figs. 2 and 3, close to the R-line wavelength of ruby ($\lambda_{em}=693$ nm), show a strong, persistent, and asymmetric feature with a line shape that is readily reproduced using the theory of Fano resonances.[19] A direct comparison of the resonance line shape, calculated for Fano parameters $Q=3$ and $\Gamma=8$ nm, is made with the 30% sample trace (from Fig. 3) in Fig. 7(a), including inhomogeneous broadening estimated to be 4 nm. The effect of inhomogeneous broadening was simulated by combining ten Fano profiles of adjustable intensities centered at fixed wavelengths (distributed evenly over the 4 nm range). The best fit result is shown as the solid curve in Fig. 7(a). The homogeneous linewidth of the 693 nm Cr^{3+} resonance [evident in Figs. 6(b) and 6(d)] was roughly $\Gamma=5$ nm, but for the ten-component simulation a value of $\Gamma=8$ nm yielded the smoothest theoretical curve and reproduced the marked asymmetry of this resonance best. Explicit wave functions were not available for the continuum defect state. Hence a first principles estimate of the line shift was unfortunately not possible.

The proximity of the 672 nm feature to the usual position of the R lines of Cr^{3+} at 693 nm in single crystals, as well as the appearance of a weak line at 693 nm in annealed

samples, indicates that trace amounts of Cr are present and that Cr^{3+} ions are involved in the resonance. Notice too that the resonance near 672 nm grows in intensity nonlinearly as the current level is increased but maintains a constant ratio with respect to the aggregate color center background emission [Fig. 7(b)]. The peak of this spectral feature, most intense at high current, is also significantly blueshifted with respect to the wavelength of the *R* line in corundum. Such a shift is readily explained with a Fano resonance as the result of coupling between the discrete and quasi-continuous states.

IV. DISCUSSION

The results presented in Figs. 2–5 show that pyrolytic synthesis readily produces point defects in alumina despite its reputation as a radiation-hard host. Defects are incorporated into the single crystal particles during kinetic synthesis and hold promise in their own right as UV sources. However, UV-C emission in the range of 240–290 nm constituted a small percentage of the overall luminescence at high currents.

The modifications of ultraviolet CL spectra that were observed to follow high current electron irradiation (Fig. 4) are consistent with charge release from neutral and ionized complexes of oxygen vacancies. In sapphire there is no prior evidence of defect migration upon high temperature annealing,[20] but excitation by various means readily changes the dynamic equilibria between different charge states of centers in alumina. In every sample subjected to high current irradiation, for example, the 520 nm emission peak exhibited a strong bleaching effect, regardless of Mg doping level. This may be ascribed to the ionization of the F_2 center, since the absorption (and therefore) density of F_2^+ centers increased during the process [Fig. 5(b)]. Despite the radiative efficiency of the ionized aggregates, no F_2^+ *emission* was directly detected, however. This was presumably because light from singly ionized centers was resonantly absorbed and reemitted by the more complex aggregates present at longer wavelengths, as shown in Figs. 3 and 4.[10]

In $Mg_xAl_{2-x}O_3$ samples, charge compensation by Mg ions on sites neighboring vacancies caused the stabilization and blueshifted emission from F^+-Mg centers. In keeping with this, a general reduction of beam-induced UV bleaching was observed as Mg concentration increased. A salient observation, however, was that at 40% Mg doping a large increase in emission intensity at wavelengths of 310 and 290 nm, attributable to a heightened concentration of F^+ and F^+-Mg centers, was observed (Fig. 4). Although F_2 centers also emit in this range when present, the absence of 520 nm emission in treated samples clearly showed that F_2 centers ionized by incident electrons did not recapture charges and neutralize reversibly after the beam treatment. Recapture of electrons by existing F^+ and F^+-Mg centers cannot result in higher densities of these centers than existed in the as-grown samples. Hence the intensification of emission around 310 nm is most likely due to the formation of new F^+ and F^+-Mg centers by the release of electrons from *F* and *F*-Mg centers to traps that are especially prevalent in 40% $Mg:Al_2O_3$ by virtue of its proximity to spinel stoichiometry.

The 40% $Mg:Al_2O_3$ LF-FSP sample was a reasonably intense ultraviolet emitter at wavelengths shorter than 350 nm. Following a brief exposure to high current levels of the electron beam, the radiative efficiency in the 250–290 nm range improved, but it never exceeded 5% of the total emission. Absorption/emission channels of defect complexes in the ultraviolet and visible range competed effectively with UV-C emission, especially at high currents. While superior performance may be achievable from simple point defects in $Mg:Al_2O_3$ by further refinement of Mg concentration in the range of 30%–50%, the use of other dopant ions (such as Ca) and thermal annealing may be the only ways to improve short wavelength emission intensities in undoped samples.

The narrow emission peak near 672 nm in powder spectra (Figs. 2–4) has an asymmetric line shape that is readily reproduced using Fano's theory [see Fig. 7(a)]. A similar feature ascribed to the coupling of Cr^{3+} *R*-line emission with a background continuum from Cr^{3+} quartet states in glasses[21] has been reported, but this particular self-interference effect and other alternative explanations are unlikely, as discussed further below. Cr^{3+} quartet states do not overlap the *R* lines in Al_2O_3. Hence a Fano interference effect could only arise from the coupling of trace Cr^{3+} impurities to quasi-continuous emission transitions of F_2^{2+} and F_2^{3+} vacancy complexes that overlap this spectral region. For this coupling to take place, the Cr and vacancy centers would have to form a composite center, in which the Cr and vacancy complex transitions can mix electronically. That is to say, the two components of a composite center exhibiting Fano resonance must occupy adjacent sites in the lattice. Hence an ionized Cr-vacancy complex is necessary to explain this feature. Direct evidence for the increase in concentration of the ionized vacancy component with increased electron beam current has already been presented in Fig. 5(b).

We now address some alternative explanations. In nanopowders, the large blueshift (with respect to the zero phonon transition of isolated Cr^{3+} at 693 nm) and broadening of the 672 nm feature could, in principle, be explained by crystal field changes in particles smaller than 100 nm (i.e., quantum size effects) or the presence of high strain fields in pyrolytically synthesized particles or Mn impurities which luminesce near this wavelength in α-phase alumina.[22] Consequently, we consider these alternative explanations below, but find that none accounts for the line shape of the 672 nm feature, its variation with Mg doping, or its proportionality to the background continuum intensity evident in Fig. 7(b).

Asymmetric line broadening and red-shifted emission of Cr^{3+} were reported earlier in disordered nanocrystalline $Cr:Al_2O_3$.[23] Broadening in this case was interpreted as the effect of disorder, and the line shape was analyzed in terms of modifications of the electron-phonon interaction in small particles. The 20 nm shift reported in the present work is to the blue, however, and comparatively large for Cr^{3+}, though not unprecedented. In alexandrite, the shortest wavelength component of the *R*-line doublet is located at 678 nm.[24] The observation of separate, unshifted Cr^{3+} lines from unstrained

sites in annealed alumina [Figs. 6(b) and 6(d)] and the intensity dependence on the color center background [Fig. 7(b)] nevertheless argue against this possibility.

Unexpected impurities might also account for the 672 nm emission in our samples. Because Mg^{2+} ions in $Mg_xAl_{2-x}O_3$ samples are effective compensators of quadrivalent species substituting for Al^{3+} at cation sites, trace amounts of extrinsic impurities such as Mn might be present. Mn^{4+} is known to emit doublet lines at 672 and 676 nm in α-Al_2O_3.[22] The presence of other charge states of manganese in the nanopowder (i.e., Mn^{2+} and Mn^{3+}) could explain the low intensity of this feature in as-grown samples [Fig. 6(a)], assuming that only a small proportion of the Mn can be charge compensated as Mn^{4+} in the as-grown material. Beam-induced ionization of Mn impurities in other sites might then account for intensification of the 672 nm feature at high current and its subsequent disappearance when the current is reduced. At lower current values, returning electrons could reasonably be assumed to restore the nonfluorescent charge states of uncompensated Mn ions. However, quantitative analysis by x-ray fluorescence placed the limit on total Mn concentration at less than 10 ppm and no evidence was ever found for doublet structure of this emission, so it seems unlikely that 672 nm emission can be ascribed to Mn^{4+} impurities.

In contrast, the pronounced asymmetry and high intensity of the 672 nm feature (upper traces of Fig. 2) are readily accounted for by quantum mechanical interference between narrow and broad transitions (Fano resonance) in an ionized Cr-F_2 composite center. In Fig. 7(a), it was shown that an inhomogeneous distribution of Fano profiles with a single pair of Q and Γ values can reproduce the observed line shape. The coupling parameters deduced from this analysis indicate strong mixing of the component eigenstates. This makes it possible to understand the intensity of the feature, since color centers have considerable oscillator strength to lend the normally forbidden R-line transitions of Cr^{3+}. Finally, the proportionality between the peak intensity of the 672 nm resonance and that of the underlying continuum emission [Fig. 7(b), solid circles and inset] is understandable in the case of a Fano resonance, since both the discrete and broadband portions of the infrared spectrum in the 672 nm region arise from one and the same center.

The final assignment of the 672 nm feature in our powder samples is therefore made to a Fano resonance of an ionized composite Cr-F_2 center. This interpretation is consistent with intensification of the 672 nm background at a superlinear rate as the F_2 feature bleaches. Bleaching of F_2 centers by ionization should increase the density of ionized Fano resonance centers, resulting in the nonlinear growth of emission, just as observed (Fig. 7(b), open squares). This in turn supports the interpretation of bleaching behavior at 520 nm as being due to ionization of F_2 centers and of the current-dependent, spectral changes at shorter wavelengths as being caused by charge migration among point defect centers.

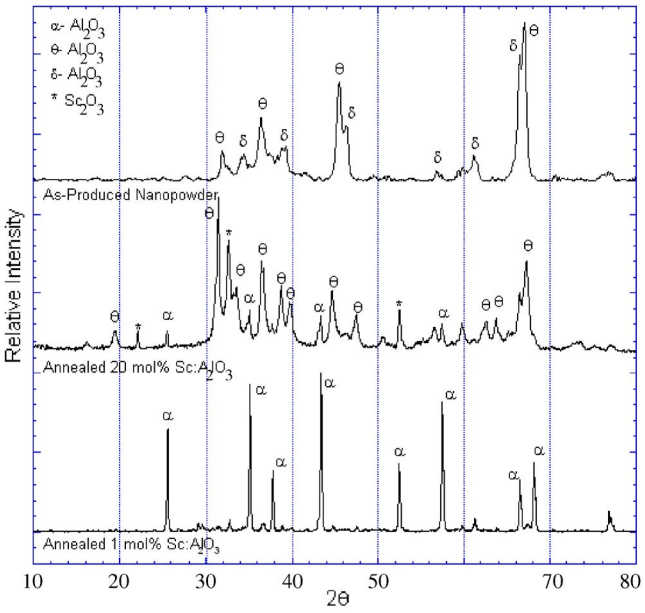

FIG. 8. (Color online) X-ray diffraction patterns of $Sc^{3+}:Al_2O_3$ nanopowders identifying the various phases of alumina that are present. The samples are unannealed 1% $Sc^{3+}:Al_2O_3$ (upper trace), 20% $Sc^{3+}:Al_2O_3$ annealed at 1200 °C (middle trace), and 1% $Sc^{3+}:Al_2O_3$ also annealed at 1200 °C (lower trace).

V. CONCLUSION

An important result of the present work is the observation that UV-C emission intensifies dramatically in $Sc^{3+}:Al_2O_3$ upon annealing above 1200 °C. The spectroscopic investigation of defect centers reported here for LF-FSP Al_2O_3 permits us to draw the conclusion that overall defect concentrations are not significantly reduced by annealing. Hence the dramatic improvement in radiative efficiency in annealed $Sc^{3+}:Al_2O_3$ samples can be attributed to the formation of α-phase alumina, as confirmed by the x-ray patterns of Fig. 8. Any notion that the improvement in emission results from some alteration in color center concentration can be eliminated by noting that in Figs. 6(b) and 6(c), the Fano resonance figures as prominently as in Figs. 2 and 3. Moreover absorption and emission energies of Sc^{3+} exceed most of the color center energy levels in alumina, so relatively little reabsorption of Sc^{3+} emission by defect centers at 275 nm would be expected to result from variations in color center concentration. Although the Sc^{3+} quantum efficiency would improve slightly if the concentration of parasitic emitters decreased, the intensification of scandium emission by two orders of magnitude upon annealing above 1200 °C cannot be explained by small changes in defect-mediated relaxation, absorption, or luminescence.

The x-ray results show very clearly that that there is essentially no α-phase alumina in as-grown powders that yields the weakest emission. There is a moderate UV-C emission from 20% annealed samples that shows a drop in δ-phase peaks and the appearance of a small proportion of α phase. Finally, the highest intensity is found to correspond to the 1% annealed samples with a composition that is almost pure α phase. We conclude that the strength of emission is

determined by the degree of crystallographic transformation to the α phase that is affected in alumina nanopowders through high temperature annealing.

Because repeated pyrolysis of alumina nanopowders synthesized by the LF-FSP method has been shown to enhance the formation of the α phase material,[13] and particle size affects the concentration of surface hydroxyl ions that quench short wavelength emission, one may assume that significant improvements over the phosphor performance reported here are possible. High concentrations of scandium may yet provide useful in enhancing UV-C emission in reprocessed nanopowders if combined with careful control of particle size.

ACKNOWLEDGMENTS

The authors acknowledge research support provided by the National Science Foundation (DMR-0502715, F014359, and CISE-0531086) and the AFOSR (F49620-03-10389).

[1]See, for example, A. R. Robertson and J. F. Fisher, in *Television Engineering Handbook*, edited by K. B. Benson (McGraw-Hill, New York, 1986).
[2]K. Kuningas, T. Rantanen, T. Ukonaho, T. Lovgren, and T. Soukka, Anal. Chem. **77**, 7348 (2005).
[3]C. H. Chuen and Y. T. Tao, Appl. Phys. Lett. **81**, 4499 (2002).
[4]R. Kinder, C. Ziegler, and J. M. Wessels, Int. J. Radiat. Biol. **71**, 561 (1997).
[5]M. Kato *et al.*, Mol. Biol. Cell **11**, 93 (2000).
[6]F. E. Regnier, B. He, S. Lin, and J. Busse, Trends Biotechnol. **17**, 101 (1999).
[7]J. D. Brewer, B. T. Jeffries, and G. P. Summers, Phys. Rev. B **22**, 4900 (1980).
[8]P. A. Kulis, M. J. Springis, I. A. Tale, V. S. Vainer, and J. A. Valbis, Phys. Status Solidi B **104**, 719 (1981).
[9]R. M. Laine, T. Hinklin, G. Williams, and S. C. Rand, Mater. Sci. Forum **343**, 500 (2000).
[10]B. D. Evans, G. J. Pogatshnik, and Y. Chen, Nucl. Instrum. Methods Phys. Res. B **91**, 258 (1994).
[11]T. T. Basiev, S. B. Mirov, and V. V. Osiko, IEEE J. Quantum Electron. **24**, 1052 (1988).
[12]N. N. Ryskin, P. Dorenbos, C. W. E. van Eijk, and S. Kh. Batygov, in *Radiation Effects and Defects in Solids* (Overseas, Amsterdam, 1995), Vol. 135, pp. 311–313.
[13]R. M. Laine, J. C. Marchal, H. P. Sun, and X. Q. Pan, Nat. Mater. **5**, 710 (2006).
[14]T. Hinklin, B. Toury, C. Gervais, F. Babonneau, J. J. Gislason, R. W. Morton, and R. M. Laine, Chem. Mater. **16**, 21 (2004).
[15]W. B. Fowler, *Physics of Color Centers* (Academic, New York, 1968).
[16]K. H. Lee and J. H. Crawford, Phys. Rev. B **15**, 4065 (1977).
[17]B. G. Draeger and G. P. Summers, Phys. Rev. B **19**, 1172 (1979).
[18]Y. Chen, M. M. Abraham, and D. F. Pedraza, Nucl. Instrum. Methods Phys. Res. B **59&60**, 1163 (1991).
[19]U. Fano, Phys. Rev. **124**, 1866 (1961).
[20]V. I. Baryshnikov, T. A. Kolesnikova, E. F. Martynovich, and L. I. Shchepina, Sov. Phys. Solid State **32**, 165 (1990).
[21]A. Lempicki, L. Andrews, S. J. Nettel, B. C. McCollum, and E. I. Solomon, Phys. Rev. Lett. **44**, 1234 (1980).
[22]A. B. Kulinkin, S. P. Feofilov, and R. I. Zakharchenya, Phys. Solid State **42**, 857 (2000).
[23]S. V. Bulyarskii, A. E. Kozhevin, S. N. Mkiov, and V. V. Prikhodko, Phys. Status Solidi A **180**, 555 (2000).
[24]J. C. Walling, H. P. Jenssen, R. C. Morris, E. W. O'Dell, and O. G. Peterson, Opt. Lett. **4**, 182 (1979).
[25]M. J. Springis and J. A. Valbis, Phys. Status Solidi B **132**, K61 (1985).
[26]M. J. Springis and J. A. Valbis, Phys. Status Solidi B **125**, K165 (1984).